DR MIRANDA ORR (Orcid ID : 0000-0002-0418-2724)

Article type : Original Paper

1. **Tau protein aggregation is associated with cellular senescence in the brain.**

2. Nicolas Musi[1,2,3,†], Joseph M. Valentine[1,†], Kathryn R. Sickora[1], Eric Baeuerle[1], Cody S. Thompson[1], Qiang Shen[4], Miranda E. Orr[1,2,3*]

3. [1]Barshop Institute for Longevity and Aging Studies, University of Texas Health Science Center at San Antonio, 15355 Lambda Drive, San Antonio, TX, 78245, USA.

[2]San Antonio Geriatric Research, Education and Clinical Center, South Texas Veterans Health Care System, 7400 Merton Minter, San Antonio, TX, 78229, USA.

[3]Glenn Biggs Institute for Alzheimer's & Neurodegenerative Diseases, 7400 Merton Minter, San Antonio, TX, 78229, USA.

[4]Research Imaging Institute, University of Texas Health Science Center San Antonio, 7703 Floyd Curl Drive, San Antonio, TX, 78229, USA.

[†]These authors contributed equally.

4. *Correspondence should be addressed to MEO orrm3@uthscsa.edu

Miranda E. Orr, PhD

Barshop Institute for Longevity and Aging Studies

15355 Lambda Drive

STCBM 2.100.05

San Antonio, TX 78245

Phone: (210) 562-6117

This article has been accepted for publication and undergone full peer review but has not been through the copyediting, typesetting, pagination and proofreading process, which may lead to differences between this version and the Version of Record. Please cite this article as doi: 10.1111/acel.12840

5. musi@uthsca.edu; jjoeyv47@gmail.com; Baeuerle@livemail.uthscsa.edu; thompsoncs@livemail.uthscsa.edu; shenQ3@uthscsa.edu

6. Tau aggregation induces cellular senescence in the brain.

7. tau, neurodegeneration, cellular senescence, aging, Alzheimer's disease, senolytic

Summary

Tau protein accumulation is the most common pathology among degenerative brain diseases, including Alzheimer's disease (AD), progressive supranuclear palsy (PSP), traumatic brain injury (TBI) and over twenty others. Tau-containing neurofibrillary tangle (NFT) accumulation is the closest correlate with cognitive decline and cell loss (Arriagada et al., 1992), yet mechanisms mediating tau toxicity are poorly understood. NFT formation does not induce apoptosis (de Calignon et al., 2009), which suggests secondary mechanisms are driving toxicity. Transcriptomic analyses of NFT-containing neurons microdissected from postmortem AD brain revealed an expression profile consistent with cellular senescence. This complex stress response induces aberrant cell cycle activity, adaptations to maintain survival, cellular remodeling, and metabolic dysfunction. Using four AD transgenic mouse models, we found that NFTs, but not Aβ plaques, display a senescence-like phenotype. *Cdkn2a* transcript level, a hallmark measure of senescence, directly correlated with brain atrophy and NFT burden in mice. This relationship extended to postmortem brain tissue from humans with PSP to indicate a phenomenon common to tau toxicity. Tau transgenic mice with late stage pathology were treated with senolytics to remove senescent cells. Despite the advanced age and disease progression, MRI brain imaging and histopathological analyses indicated a reduction in total NFT density, neuron loss and ventricular enlargement. Collectively, these findings indicate a strong association between the presence of NFTs and cellular

senescence in the brain, which contributes to neurodegeneration. Given the prevalence of tau protein deposition among neurodegenerative diseases, these findings have broad implications for understanding, and potentially treating, dozens of brain diseases.

INTRODUCTION

The underlying processes driving chronic neurodegeneration in Alzheimer's disease (AD) and related neurodegenerative disorders are largely unknown and disease-modifying treatments remain elusive. The accumulation of tau protein is the most common pathology among these diseases making tau an appealing molecular target for intervention (Orr et al., 2017). Tau-containing neurofibrillary tangles (NFTs) closely track with disease severity in human AD ((Arriagada et al., 1992); however, NFT-containing neurons are long-lived and do not induce immediate cell death (de Calignon et al., 2009). *In silico* modeling predicts that NFT-containing neurons may survive decades (Morsch et al., 1999), which suggests that non-cell autonomous mechanisms may contribute to NFT-associated toxicity.

Experimental data from various studies indicate that tau pathology may be associated with cellular senescence, a fundamental aging mechanism shown to contribute to several chronic diseases (recent review Kirkland and Tchkonia, 2017). This complex stress response induces a near permanent cell cycle arrest, adaptations to maintain survival, cellular remodeling, metabolic dysfunction and disruption to surrounding tissue to the secretion of toxic molecules (Childs et al., 2016). While many of these features have been described in AD brains and transgenic animal models throughout the literature (e.g., aberrant cell cycle activity, $p16^{INK4A}$ co-localization with NFTs (Arendt et al., 1996), decreased lamin B1, heterochromatin relaxation (Frost et al., 2016), etc.,); a role for cellular senescence in neurodegeneration has not been investigated. We hypothesized that tau accumulation may activate this stress response, and thereby initiate a chronic degenerative

process culminating in neuron loss and brain dysfunction. To test this hypothesis, we examined human brain tissue with NFT pathology and utilized AD transgenic mouse models that develop tau-associated pathologies. Also, we employed methods to genetically reduce NFTs and pharmacologically clear senescent cells. Our results indicate that NFTs induce cellular senescence in transgenic mice and postmortem human brain tissue. We also found that senolytics decreased cortical NFT burden, brain atrophy and neuron loss in an advanced age (20-mo-old) transgenic mouse model of tau-associated neurodegeneration.

RESULTS

NFT-bearing neurons from postmortem AD brain tissue displayed a senescence-like transcriptomic profile

We queried the publicly available GEO Profiles database (Barrett et al., 2013) for gene sets specific to NFTs. We evaluated laser capture microdissected cortical neurons containing NFTs from AD brains (GEO accession GDS2795) and compared them to adjacent histopathologically normal neurons for a within-subjects study design (Dunckley et al., 2006). NFT containing neurons upregulated genes involved in cell survival and viability, inflammation, cell cycle progression and molecular transport and downregulated apoptosis, necrosis and cell death pathways (Figure 1a). NFκB, a pro-survival master transcriptional regulator of inflammation, was the highest predicted upstream regulator of the NFT-gene expression profile. In agreement with inflammatory activation, other predicted upstream regulators included IFNG, TNF, TLR4, IL1B and CXCL1 (Figure 1b). Collectively, the molecular pathways identified in the NFT analyses resembled cellular senescence.

NFTs were associated with a senescence-associated transcriptomic profile in tau transgenic mice

We used the rTg(tau_{P301L})4510 transgenic mouse line, hereon referred to as "tau_{NFT}" to investigate a link between NFT formation and a senescence-like phenomenon in neurodegeneration. These mice develop well-characterized, aggressive, tau pathology in forebrain regions concomitant with neurodegeneration and cognitive deficits (Santacruz et al., 2005) (pathology illustrated in Figure S1). Mice that overexpress wild type human tau, "tau_{WT}," express the same level of transgene as tau_{NFT}, but acquire age-dependent tau pathogenesis at a much slower rate and are used to identify effects of elevated pre-pathogenic tau (Hoover et al., 2010) (Figures S1 and S2); age-matched tau_{NFT} littermate mice without human tau overexpression serve as wild type controls, "CTL". To determine if NFT containing neurons in mice induced a gene expression profile resembling cellular senescence, we assessed hippocampal gene expression patterns in tau_{NFT} mice before (~2-month-old) and after (~6-month-old) NFT formation (GSE56772). Consistent with NFTs from human AD, mouse NFTs also caused significant activation scores for IFNG, TNF, IL-1B, as well as enrichment in other senescence associated JAK, STAT, CDKN2A and BCL2 predicted upstream regulators (Figure 1c) indicating translational relevance for using tau_{NFT} mice to explore our hypothesis.

Evidence of DNA damage, SASP and NFκB activation were associated with NFTs

Senescence-inducing stressors often inflict DNA-damage that drives production of the SASP (Rodier et al., 2009). Tau_{NFT} mouse brains displayed significantly elevated histone γ-H2ax, a sensitive marker of both double-stranded DNA breaks and cellular senescence (Sedelnikova et al., 2004) (P = 0.0056; Figure 1d-e). The cell cycle protein p21, encoded by *Cdkn1a,* is upregulated in many senescent cell types and has been associated with DNA damage during neuronal aging (Jurk et al., 2012). Similarly, elevated expression of the cyclin

dependent kinase inhibitor 2a, *Cdkn2a,* is one of the most robust markers of cellular senescence, and its protein product, $p16^{INK4A}$, co-localizes with NFTs in human AD (Arendt et al., 1996). Because anti-p21 and anti-$p16^{INK4A}$ antibodies are notoriously poor in mouse tissue, we exclusively measured *Cdkn1a* and *Cdkn2a* gene expression. Tau_{NFT} brains expressed 3-fold higher *Cdkn1a* than control mice (P = 0.0178, Figure 1f), which was replicated in a separate mouse cohort (P = 0.0086*,* Figure S1f). Moreover, *Cdkn2a* was expressed at levels 2.7- and 2.6-fold higher in tau_{NFT} than CTL and tau_{WT}, respectively (P = 0.0303 and P = 0.0352, respectively; Figure 1g); this effect was replicated in an independent mouse cohort (P = 0.0016, Figure S1g).

Senescent cells exert chronic tissue degeneration through secretion of toxic SASP (Coppe et al., 2010). Consistent with the transcriptomic profile in human NFT-bearing neurons and mouse brain tissue (Figure 1a-c), SASP genes were found to be upregulated in tau_{NFT} brains, i.e., *Il1b* was 4- and 2-fold higher than CTL and tau_{WT}, respectively; and *Cxcl1* was 4-fold higher than both control genotypes; *Tnfa* was 13- and 8-fold higher than CTL and tau_{WT}, respectively; *Tlr4* was 3-fold higher than both control genotypes (Figure 2a-d). Further gene expression analyses allowed us to define an array specific to tau-pathology in tau_{NFT} brains (Figure S2e). NFκB regulates the pro-survival, pro-inflammatory SASP gene expression profile characteristic of cellular senescence (Salminen & Kaarniranta, 2011). Consistent with NFκB pathway activation and the SASP profile, nuclear localized NFκB p65 was significantly increased in tau_{NFT} brains (Figure 2e-f). In all measures, tau_{WT} mice were not significantly different from CTL. These results suggest that insoluble tau and/or post-translational modifications associated with insoluble tau, but not general tau overexpression, were responsible for the senescence-associated response (i.e., DNA damage, NFκB activation and upregulated SASP; Figures 1 and S2).

SA β-gal activity did not correlate with NFTs or brain atrophy.

In regenerative tissues and *in vitro* cultures, senescent cells may exhibit SA β-gal activity, which is a measure of lysosomal galactoside activity at pH 6.0 and indicative of altered/expanded lysosomal compartments (Severino et al., 2000). Examination of the gene that codes for the hydrolase enzyme, galactosidase beta (β) 1 (*Glb1*), revealed that tau_{NFT} mice expressed higher *Glb1* gene expression than controls (Figure S3). However, staining for β–gal hydrolase activity at pH 6.0 revealed fewer positive cells than controls. Further, SA β–□al reactive cells were observed even in very young mice (1-month-old) and the number of SA β–gal reactive cells was positively correlated with brain mass (R^2: 0.4852, P = 0.0039 Figure S3). While our results indicate that SA β–gal reactivity did not correlate with other senescence markers or brain atrophy, the observed increase in *Glb1* gene expression along with a decrease in lysosomal activity at pH 6.0, compared to controls, is suggestive of tau-associated lysosomal defects, which has been reported by others (Caballero et al., 2018; Y. Wang et al., 2009).

NFT-containing brain tissue displayed aberrant cellular bioenergetics

Mitochondrial dysfunction is obligatory for SASP production and cellular senescence (Correia-Melo et al., 2016; Hutter et al., 2004). To examine mitochondrial bioenergetics, we performed high-resolution respirometry to yield accurate quantitative measurements of oxidative phosphorylation in response to specific substrates for complex I, complex II, fat oxidation and electron-transfer system (ETS) capacity. Across genotypes, we compared cortex, hippocampus and cerebellum. This allowed for evaluation of specific differences in oxygen consumption due to elevated transgenic tau (comparing CTL with tau_{wt} and tau_{NFT}), pathogenic tau specific effects (comparing tau_{wt} to tau_{NFT}), as well as the interaction among brains regions and tau expression (e.g., cortex and hippocampus express transgenic tau and

develop NFTs, but cerebellum does not). We found a significant genotype main effect for oxygen flux in both cortex and hippocampus, indicating that global respiratory capacity was impaired in NFT containing brain regions ($P < 0.0001$; Figure 3), an effect primarily driven by CI+CII respiration coupled to ATP production (cortex: $P = 0.0034$; hippocampus: $P = 0.0215$; Figure 2g and h, respectively), and uncoupled or maximum respiratory capacity (cortex: $P = 0.0248$; hippocampus: $P = 0.0261$; Figure 3g and h, respectively). These changes were different between tau_{NFT} and each of the control mouse lines, CTL and tau_{WT} mice. Because tau_{WT} and tau_{NFT} mice express comparable total tau levels, alterations to respiratory capacity cannot be attributed to tau overexpression. Citrate synthase activity is a surrogate marker of total mitochondrial content/mass, and was similar across genotypes and brain regions (Figure 3i) suggesting that the defects in cellular respiration were due to altered mitochondrial quality, not content/mass. Moreover, tau_{NFT} cerebellum did not show deficits in cellular respiration or *Cdkn2a* upregulation (Figure 3j, k), indicating that senescence-associated mitochondrial dysfunction was present only in brain regions with persistent pathogenic tau expression.

Cdkn2a upregulation occurred with NFT onset and correlated with NFT density

We pursued multiple genetic approaches to determine whether senescence was mechanistically linked to NFT density, NFT onset, or merely protein accumulation. Reducing NFT load in age-matched animals is not feasible; once NFTs form, they cannot be therapeutically eliminated. However, genetically ablating endogenous mouse tau (microtubule associated protein tau, *Mapt*) reduces NFT pathology and neurodegeneration in tau_{NFT} mice (tau_{NFT}-$Mapt^{0/0}$) (Wegmann et al., 2015). The reduced tau pathology corresponded with 60% lower *Cdkn2a* expression ($P = 0.0041$, Figure 4a), decreased SASP (Figure S4) and decreased brain atrophy (tau_{NFT}-$Mapt^{0/0}$: 0.4058 ± 0.009 versus age-matched tau_{NFT} $Mapt^{wt/wt}$: 0.3451 ± 0.0116; 17.5% difference, $P = 0.0143$, Figure 4b). Tau_{NFT}

mice develop aggressive tauopathy with NFT formation in early life, and show a senescence-associated transcriptomic profile with NFT onset (Figure 1c). To detect subtle cellular changes associated with different stages of age-associated NFT development and progression, we focused on tau_{WT} mice between 16-28-months-old. *Cdkn2a* gene expression increased significantly during this age interval, and at 28 months of age tau_{WT} *Cdkn2a* expression was similar to that of 16-month-old tau_{NFT} mice (Figure 4c). Concomitantly, at this age, tau_{WT} mice developed NFTs as visualized by Bielschowsky silver staining and immunofluorescence analyses (Figure 4d). These results provide additional evidence for the association between NFT formation and senescence-associated *Cdkn2a* upregulation.

Cdkn2a upregulation was specific to NFT tau pathology and correlated with brain atrophy

To determine if *Cdkn2a* expression was driven specifically by NFTs, or whether AD-associated Aβ protein deposition also increased *Cdkn2a*, we utilized 3xTgAD mice that acquire both AD-associated pathologies with Aβ deposition and NFT onset at 6 and 18-months of age, respectively (Oddo et al., 2003). In 15-month-old mice with heavy Aβ deposition and phosphorylated tau, but lacking NFT pathology (Orr et al., 2014), *Cdkn2a* expression was not elevated (Figure 4e). These data indicate that *Cdkn2a* expression was neither a response to general protein accumulation, nor to pre-NFT tau pathology, but instead required the presence of NFTs. Further, when plotted against brain weight, *Cdkn2a* expression was a strong predictor of brain atrophy across mouse lines ($P < 0.0001$, $R^2 = 0.5615$; Figure 4f).

CDKN2A was upregulated in NFT-containing brains from patients with progressive supranuclear palsy

Tau pathology is common among >20 brain diseases. To investigate whether the findings in human AD neurons and transgenic mice translated to human brains with pure tauopathy (i.e., NFT pathology without other protein aggregates such as Aβ), we acquired human brain tissue with histopathologically confirmed progressive supranuclear palsy (PSP) (Table 1 for patient characteristics). PSP is an age-associated tauopathy that clinically manifests as parkinsonism with additional motor abnormalities and cognitive dysfunction (Orr et al., 2017), and is neuropathologically defined by accumulation of four-repeat (4R) tau, NFTs, gliosis and neurodegeneration (Flament et al., 1991). Consistent with the results from transgenic mice, *CDKN2A* was upregulated in PSP brains (P = 0.0415, Figure 4g) and expression correlated with NFT deposition, specifically in the parietal lobe (ANOVA, P = 0.0008; Kendall's Tau rank correlation P = 0.059, Figure 4h). Moreover, one individual with the worst cognitive performance, Mini–Mental State Examination (MMSE) score of 12, displayed the highest level of *CDKN2A* expression, and high molecular weight tau (Figure 4i). Collectively, these findings led us to conclude that NFTs were directly linked to senescence-associated *Cdkn2a* upregulation, which in turn was a strong predictor of neurodegeneration and cognitive decline.

Senolytic treatment reduced NFT burden and neurodegeneration

Senescent cells comprise a small proportion of total cellular makeup within a tissue (~15%) (Herbig et al., 2006). Nonetheless, genetically (Baker et al., 2011) or pharmacologically (Zhu et al., 2015) clearing even a small percentage of these cells improves healthspan and delays age-associated diseases (Kirkland et al., 2017). We used some of the best-characterized senolytics to date, dasatinib and quercetin (DQ), to determine the utility of targeting cellular senescence to treat tau-associated

neurodegeneration in late-life. Beginning at 20-months-old, tau_{NFT}-*Mapt*$^{0/0}$ and non-transgenic-*Mapt*$^{0/0}$ mice were randomized to receive vehicle or DQ at bi-weekly intervals for 3 months. When mice were 23-months-old, brain structure and cerebral blood flow were analyzed with MRI and postmortem histopathology (Figure 5 and S5). Consistent with senescent cell removal, intermittent DQ treatment significantly reduced the number of NFT-containing cortical neurons ($P < 0.0001$, 5% reduction; Figure 5a,b). Relative to the existing neuronal population at this advanced age, gene expression of the NFT-associated senescence gene array was reduced by DQ ($P = 0.0006$; Figure S6a). Among these genes, those highly sensitive to NFT-dependent upregulation (Data S2) were most affected to NFT removal by DQ (i.e., *Tlr4:* $P = 0.0459$ *and Cxcl1:* $P = 0.0142$*;* Figure 5c; S6*)*. NFTs are highly correlated with the rate of ventricular enlargement, an indicator of brain atrophy and hallmark of AD pathology (Silbert et al., 2003). Tau_{NFT} mice recapitulate this pathology on a wild type (Figure S1) and *Mapt*$^{0/0}$ background ($P = 0.0007$; Figure 5d). The DQ-dependent reduction in cortical NFTs corresponded with decreased ventricular volume pathology (28% decrease, $P = 0.05$, Figure 5d, f) and a reduction in cortical brain atrophy (compared to controls: $P = 0.0092$ and $P = 0.0274$, vehicle and DQ, respectively; Figure S5a). The absence of a full rescue of ventricular enlargement to that of control animals was not completely unexpected considering the severity of disease and age of the animals when treatment was initiated.

The MRI images also revealed white matter hyperintensity (WMH) pathology, areas of increased brightness on T2-weighted MRIs (Figure S5b, c). WMH is driven by cerebral small vessel disease, which causes chronic ischemia and increased risk of cognitive decline and dementia (reviewed, (Prins & Scheltens, 2015)). Tau_{NFT}-*Mapt*$^{0/0}$ vehicle-treated mice displayed significant WMH pathology ($P = 0.0341$; Figure S5b, c), which is consistent with recent reports of NFT-induced vascular abnormalities (Bennett et al., 2018). However, tau_{NFT}-*Mapt*$^{0/0}$ mice treated with DQ did not display WMH volumes statistically different than control mice ($P = 0.2458$; Figure S5b, c). Aberrant cerebral blood flow is a functional defect that occurs in AD and tau_{NFT} mice, and is closely associated with cognitive impairment (Wells

et al., 2015). In brain tissue with tau pathology, cerebral blood flow was elevated in tau_{NFT} *Mapt*$^{0/0}$ vehicle-treated mice (21% whole brain, $P = 0.045$; cortex, 48.7%, $P = 0.051$, Figure S5d, e), and consistent with previous reports of tau_{NFT} mice on a *Mapt*$^{+/+}$ background (Wells et al., 2015). DQ improved cerebral blood flow in tau_{NFT} *Mapt*$^{0/0}$ mice such that cerebral blood flow was no longer statistically different from controls (Figure S5d, e). Overall, a composite analysis of DQ treatment in tau_{NFT} mice revealed a significant global benefit on cerebral blood flow and neurodegeneration ($P = 0.0138$; Figure S5f).

To elucidate whether the DQ-dependent reduction in NFT burden, SASP expression and improvements to brain structure and cerebral blood flow conferred neuroprotection, we measured levels of cell-type specific protein expression in the brain. DQ-treated mice expressed significantly higher levels of neuronal proteins (NeuN: 25%, synaptophysin: 40.8%; PSD95: 38.5%; $P < 0.05$; Figure 5f-i). The astrocyte protein GFAP was unchanged, while microglia Iba1 expression was elevated (Iba1: 40%, $P = 0.0013$; Figure S6b-d) suggesting that DQ-mediated neuroprotection and decreased SASP was not derived from a reduction in pro-inflammatory glia (astrocytes or microglia) but instead associated with fewer NFT-containing neurons. Moreover, DQ did not alter total human tau protein levels indicating the effects were not driven by changes in tau protein expression, but rather insoluble NFTs or associated post-translational modifications (Figure S7). Collectively, our data suggest that cyclic senescent cell removal of NFTs with DQ produced long-lasting global effects on brain, as evidenced by histopathology and MRI analyses.

Discussion

The inability to effectively treat tau-associated diseases arises, in part, from a limited understanding of processes driving neurodegeneration during the prodromal period. We have identified cellular senescence, the quintessence of latent tissue degeneration, as a

cellular mechanism upregulated in tau-associated neurodegeneration. Findings in NFT-developing transgenic mice, postmortem human AD and PSP brain tissue support this concept.

Cellular senescence is an elaborate stress response that varies across tissues, and even among cell types within tissues. Our experimental data provide an initial report of features consistent with cellular senescence in the brain (i.e., transcriptomics, upregulated *Cdkn1a* and *Cdkn1a*, SASP molecules and altered cellular bioenergetics). A complete depiction of tau-associated cellular senescence will require several follow-up studies guided by these results, and a close evaluation of already published data. For example, a cursory search of literature has revealed aberrant HMGB1 (Nilson et al., 2017); loss of lamin B and heterochromatin relaxation (Frost et al., 2016); and altered cellular morphology (Orr et al., 2012) associated with tau pathology; all of which are consistent with cellular senescence.

Tau processing is complex and requires tight regulation to maintain neuronal viability. Alterations to tau splice variant expression, post-translational modifications (e.g., phosphorylation, acetylation, glycosylation, conformational changes, oligomerization, cleavage, etc), subcellular localization, etc., may result in neuronal dysfunction. As such, pathogenic tau is observed in a spectrum of neurodegenerative diseases where its histopathological characterization aids in clinical diagnoses. Our experimental results have revealed a strong association between NFT pathology and a senescence-like phenotype. However, we cannot exclude the possibility that other tau species and/or specific post-translational modifications may also contribute to cellular senescence. The upstream mediators driving tau-associated cellular senescence in AD and PSP also remain unknown; however, it is tempting to speculate that tau-induced cell cycle re-entry may be involved (Arendt, 2012). Aberrant cell cycle re-entry causes neuronal apoptosis and AD-associated pathology (Park et al., 2007), and requires soluble tau (Seward et al., 2013). The observed increase in NFT-associated *Cdkn1a* and *Cdkn2a* gene expression may allow stressed neurons to abort cell cycle re-entry and enter a cellular state similar to cellular senescence.

In this way, NFTs formed in early pathogenic stages due to acute stress may initially protect neurons from cell death, but then contribute to neurodegeneration later in life through senescence-like mechanisms by altering the bioenergetic state of the brain and upregulating the toxic SASP.

Pathogenic tau induces a traditional neuroinflammatory response by activating microglia and astrocytes (for recent review (Laurent et al., 2018)). Our data suggest that NFT-containing neurons may be active participants in perpetuating the inflammatory response as well. Future studies are required to better understand the contribution of SASP to the overall neuroinflammation phenotype common among many brain diseases. Nonetheless, our findings suggest that therapeutically targeting cellular senescence effectively interrupted a chronic neurodegenerative cascade to decrease NFT-associated pathology and improve brain structure and aberrant cerebral blood flow even in the presence of established tau pathology in a late-life advanced disease state. Overall our data provide evidence that cellular senescence may be an underlying pathogenic process common among tauopathies, which opens a new field of investigative research and offers a potential druggable target to treat the >20 tau-associated neurodegenerative diseases.

METHODS

Mice. All animal experiments were carried out following National Institutes of Health and University of Texas Health Science Center at San Antonio (UTHSCSA) Institutional Animal Care and Use Committee guidelines. We used 16 to 32-month-old male and female rTg4510 and rTg21221 mice that reversibly express P301L mutant human tau or wild type human tau 4R02, respectively, on either a wild type or *Mapt* knockout Bl6/FVB genetic background (Hoover et al., 2010; Santacruz et al., 2005; Wegmann et al., 2015). Non-transgene expressing littermates from rTg4510 and rTg21221 are used as controls; since no differences were found between these control lines, only littermates from rTg4510 are used here (Extended Data Figure 1f-i). The mice were bred by Rose Pitstick and George A.

Carlson at McLaughlin Research Institute, Great Falls, MT. Mouse euthanasia, brain dissection and preparation was performed as previously described (Orr et al., 2012; Orr et al., 2014).

Ingenuity Pathway Analyses (IPA). The GEO accessions GDS2795 and GSE56772 were accessed from the GEO Profiles database (Barrett et al., 2013; Dunckley et al., 2006) with Rstudio version 1.0.143. Because the GDS2795 datset was a within subjects design, ratios of NFT vs CTL gene expression were generated for each subject. Mean ratios of each gene from GDS2795 and fold change values from GSE56772 were uploaded into IPA software (IPA, QIAGEN Inc.,https://www.qiagenbioinformatics.com/products/ingenuity-pathway-analysis). For GDS2795 GeneBank Accession IDs were used and 34910 out of 54675 genes were identified by IPA software. The expression fold change cutoff value was set at 3 (both down/upregulated) compressing the analyses to 3048 genes. For GSE56772 LIMMA package was used to determine fold change and p-values. The *P*-value cutoff for IPA analysis was set at $P < 0.01$ yielding 1294 transcripts, 738 down- and 556 up-regulated. We utilized IPA causal analytic tools(Kramer et al., 2014) to elucidate predicted upstream regulators, as well as disease and biological functions with significant z-scores enriched in our data set.

Findings from GDS2795 were replicated with more stringent criteria ($p < 0.05$ for NFT/CTL ratios with no fold change limit) allowing for 1715 genes to be uploaded into IPA with similar results. Similarly, these findings were replicated a third time using the LIMMA package, the most common method for microarray analysis. This method did not take into account within subjects design. Using a $P < 0.05$, 1219 differentially regulated genes were uploaded for IPA analyses; the results were similar to the original findings. Furthermore, results from GSE56772 were replicated using Gene Set Enrichment Analysis (GSEA) with default setting and similar results were obtained.

RNA extraction and qPCR. Frozen forebrain and cerebellum were powdered in liquid nitrogen. RNA was extracted from ~25mg of each respective brain (or brain region) using the RNAqueous 4PCR® kit (Ambion), following the manufacturer protocol including the 15 minute DNase treatment. qPCR was performed on 25ng RNA using the TaqMan® RNA-to-CT™ 1-step kit. All gene expression analyses were made using Taqman gene expression assays. RNA Polymerase II Subunit J (Polr2j) expression was used as an internal control for both mouse and human gene expression assays, Mm00448649_m1 and Hs01558819_m1, respectively. Taqman genes expression identifiers for target genes are as follows: mouse and human *Cdkn2a*: Mm00494449_m1 and Hs00923894_m1, respectively; other mouse genes: *Cdkn1a:* Mm00432448_m1*; Glb1:* Mm01259108_m1*; Cxcl1:* Mm04207460_m1; *Tlr4*: Rn00569848_m1; *Il1β*: Mm00434228_m1; *TNF*: Mm00443258_m1. The senescent cell population comprises a small proportion of all cells in a tissue; therefore SASP gene expression values were normalized to neuronal *Mapt,* the senescence-susceptible neuronal population. qPCR was performed using the Applied Biosystems 7900HT Sequence Detection System, with SDS software version 2.3. Cycle profile was performed using the kit manufacturer protocol.

Protein extraction and capillary electrophoresis. 50mg frozen forebrain was used for subcellular fractionation and capillary electrophoresis as previously described (Orr et al., 2015; Orr et al., 2014). Briefly, frozen tissue was powdered in liquid nitrogen, then homogenized with dounce and pestle and fractionated following manufacture protocol (Subcellular Protein Fractionation Kit, ThermoFisher Scientific, USA). Protein concentrations were determined with BCA (Biorad, USA); 2ug protein was used for capillary electrophoresis. Antibodies were diluted in Wes Antibody Diluent to the final working concentrations: p65, 1:50 (Cell Signaling, D14E12; Beverly, MA, USA); phospho-Ser139 H2A.X, 1:50 (Cell Signaling, 20E3; Beverly, MA, USA); HT7, 1:1000 (Pierce/Invitrogen, USA); NeuN, 1:50 (Millipore, MAB377; Temecula, CA, USA): GFAP 1:200 (Cell Signaling, D1F4Q; Beverly, MA, USA); synaptophysin, 1:50 (Cell Signaling, D35E4; Beverly, MA,

USA); Plp1, 1:100 (Sigma, HPA004128; St. Louis, MO, USA). See Supporting Data Table 1 for complete antibody information. Protein quantification was performed by normalizing to total protein concentration (Li & Shen, 2013; Moritz, 2017); (Extended Data Figure 8).

Histology. Brains were fixed in 4% PFA for 48 hours, transferred to PBS containing 0.02% sodium azide and vibratome sectioned at 30μm. Sections were washed 3x with TBS (pH 7.4), and incubated in 50% ethanol for 5 mins; followed by 70% ethanol for 5 minutes. The sections were then submerged in 0.7% sudan black b dissolved in 70% ethanol for 5 minutes to quench lipofuscin-like autofluorescence. Tissues were then rinsed 3 times for 1-2 min in 50% ethanol. Following this step, tissue sections were transferred from 50% ethanol to TBS and proceeded to immunofluorescence staining as described previously(Orr et al., 2015; Orr et al., 2014). Primary antibodies used: PHF1 (1:100, kind gift from Dr. Peter Davies), NeuN (1: 500 Cell Signaling, D3S31; Beverly, MA, USA), Histone 3 (1:400, Cell Signaling, D1H2; Beverly, MA, USA) (Extended Data Table 1). Secondary antibodies: Goat anti-Mouse IgG (H+L), Alexa Fluor 594 and Goat anti-Rabbit IgG (H+L), Alexa Fluor 488 (1:1500, Thermo Fisher Scientific). Imaging was performed using a Zeiss LSM 780 confocal microscope, with ZEN 2.3 software.

Confocal Image Analyses: Image analyses were conducted using ImageJ's FIJI. Analyses were performed on confocal z-stacks imaged at 40x magnification. A maximum intensity image was created by compressing four z-stack planes. All analyzed DAPI fields were applied a bandpass filter under the same conditions, applied a threshold, and measured using particle analysis excluding particles smaller than 25 μm^2. All particles measured in the analysis were checked for mislabels and any particles that included 2 nuclei or exhibited abnormal/incorrect selection were excluded from analysis. Cell type was identified using NeuN (neurons) and PHF1 (NFT-bearing neurons) immunofluorescence.

SA β-gal Staining: Following euthanasia, brains were immediately removed and fresh-frozen in an isopentane/liquid nitrogen slurry. The frozen brains were immediately adhered to the cryotome chuck with optimal cutting temperature compound (OCT) pre-cooled to -

18°C; 10μm coronal sections were collected, and mounted on superfrost plus microscope slides (FisherScientific). After sectioning, slides were fixed for 10 minutes in 2% paraformaldehyde/0.2% glutaraldehyde at room temperature, rinsed 3x in TBS and stained with SA β–gal staining solution overnight(Dimri et al., 1995). Following SA β–gal staining, sections were processed for immunofluorescence as described above.

Brightfield/SA β–gal Counts: SA β–gal brightfield images were taken on a Nikon Eclipse Ci-L microscope, with a digital site DS-U2 camera (NIS-Elements software BR 4.51.00). Coronally sectioned mouse brains (10μm) were evaluated using DAPI, SA β–gal positive and negative cells in the CA2 region of the hippocampus were counted across 8 tissue sections per animal (n=5 per genotype). Staining was considered positive when granules of blue stain were present.

High Resolution Respirometry. HRR was conducted using two Oxygraph-2k (model D & G) machines from Oroboros Instruments (Austria). To minimize mitochondrial damage associated with mitochondrial isolation techniques, we measured oxygen consumption in fresh brain tissue homogenates(Makrecka-Kuka et al., 2015). Whole hippocampus, cortex and cerebellum were homogenized with ~15 strokes using a Kontes glass homogenizer in 5% w/v ice cold MiRO6. Two mg of brain homogenate were loaded into the chamber and experiments were carried out when oxygen concentration in each well was saturated under atmospheric conditions (~190nM/mL O_2). All reagents and SUIT protocol were described previously(Pesta et al., 2011) with small modifications. Briefly, 1.25mM ADP was sufficient for saturation in brain homogenate, rotenone was added at a concentration of 1μM, and FCCP was added in a single injection at a concentration of 0.5μM.

DQ administration: Control and tau_{NFT} *Mapt*$^{0/0}$ mice aged 19-20 months were randomized to receive DQ senolytic (5mg/kg dasatinib (LC Laboratories, Woburn, MA) with 50mg/kg quercetin (Sigma-Aldrich, St. Louis, MO)) or vehicle (60% Phosal 50 PG, 30% PEG 400, and 10% ethanol) via oral gavage as described previously(Ogrodnik et al., 2017). Mice were

weighed and fasted for 2 hours prior to treatment. One month after the first treatment, senolytic or vehicle gavage continued on a bi-weekly basis for a total of six treatment sessions over twelve weeks. Within two weeks of the final treatment, all mice underwent MRI analyses.

MRI: MRI experiments were performed on an 11.7 Tesla scanner (Biospec, Bruker, Billerica, MA). A surface coil was used for brain imaging and a heart coil(Muir et al., 2008) for arterial-spin labeling. Coil-to-coil electromagnetic interaction was actively decoupled. Mice were maintained on 1.5% isoflurane anesthesia for MRI duration. *Anatomical MRI*: Anatomical images were obtained using a fast spin echo sequence with a matrix = 128x128, field of view (FOV) = 1.28cmx1.28 cm, repetition time (TR) = 4000 ms, effective echo times = 25 ms. Thirty 1-mm coronal images were acquired with 4 averages. Total scan time= 8.5 minutes. *Cerebral blood flow (CBF)* was measured using continuous arterial spin labeling technique with single shot, spin-echo, echo-planar imaging and analyzed as previously described(Shen et al., 2015). The images were acquired with partial Fourier (3/4) acquisition, matrix size = 64×64, FOV = 1.28cmx1.28 cm, TR = 3000 ms, TE = 10.59 ms, post labeling delay=350ms. Seven 1-mm coronal images were acquired with 100 repetitions. Total scan time=10 mins. *Analyses:* MRI analysis was conducted using Stimulate (Center for Magnetic Resonance Research, University of Minnesota Medical School, Minneapolis, MN) running on a CentOS5 Linux Operating System(Strupp). Anatomical MRI images were used to measure cortex, subcortex, ventricle, white matter hyperintensities (WMH) and whole brain volume. The desired Region of Interest (ROIs) were outlined and volumes were obtained by multiplying ROI total voxels by voxel volume (0.004 mm^3). Ventricle and WMH volume was obtained by thresholding anatomical image voxels to highlight regions of greater intensity, followed by ROI traces of the target regions. Whole brain volume was obtained by ROI trace after removal of the skull using a local Gaussian distribution 3D segmentation MATLAB code (L. Wang et al., 2009).

Statistical Measures. Transgenic mouse analyses: Measurements were taken from distinct samples. Key finding were repeated in separate mouse cohorts and are listed in Extended Data Figures. Each age cohort for all analyses contained 3–9 animals (specified in figure legends); both males and females were included. Only females were included in DQ treatment and MRI analyses due to animal availability. Statistics were not used to predetermine sample sizes, but instead was determined empirically from previous experimental experience with similar assays, and/or from sizes generally employed in the field. Data are expressed as mean ± standard error of the mean (s.e.m.). Genotype and treatment comparisons were analyzed using one-way analysis of variance (ANOVA) with Tukey post-hoc, or unpaired t-test unless stated otherwise in the figure legends. Respirometric data, brain volume and cerebral blood flow data were analyzed using two-way ANOVAs (genotype x respirometric parameter) and (treatment x brain region), respectively, with Tukey's post hoc comparisons. **Human PSP brain tissue analyses**: the PSP group contained 14 samples and were compared to 10 age-matched controls with both sexes included; significance was determined with unpaired two-tailed t-test. We performed ANOVA analysis of the log base 10 transformed CDKN2A expression as predicted by the levels of AD pathology, in addition we used the more conservative Kendall's Tau rank correlation to test this association as well. The human CDKN2A and AD pathology analyses were performed using the R v3+ (Vienna, Austria) environment for statistical computing using an accountable data analysis process. All other data were analyzed using GraphPad Prism version 7.0c for Mac OS X, GraphPad Software, San Diego California, USA, www.graphpad.com/. Data were considered statistically different at $P < 0.05$.

Arendt, T. (2012). Cell cycle activation and aneuploid neurons in Alzheimer's disease. *Mol Neurobiol, 46*(1), 125-135. doi:10.1007/s12035-012-8262-0

Arendt, T., Rodel, L., Gartner, U., & Holzer, M. (1996). Expression of the cyclin-dependent kinase inhibitor p16 in Alzheimer's disease. *Neuroreport, 7*(18), 3047-3049.

Arriagada, P. V., Growdon, J. H., Hedley-Whyte, E. T., & Hyman, B. T. (1992). Neurofibrillary tangles but not senile plaques parallel duration and severity of Alzheimer's disease. *Neurology, 42*(3 Pt 1), 631-639.

Baker, D. J., Wijshake, T., Tchkonia, T., LeBrasseur, N. K., Childs, B. G., van de Sluis, B., . . . van Deursen, J. M. (2011). Clearance of p16Ink4a-positive senescent cells delays ageing-associated disorders. *Nature, 479*(7372), 232-236. doi:10.1038/nature10600

Barrett, T., Wilhite, S. E., Ledoux, P., Evangelista, C., Kim, I. F., Tomashevsky, M., . . . Soboleva, A. (2013). NCBI GEO: archive for functional genomics data sets--update. *Nucleic Acids Res, 41*(Database issue), D991-995. doi:10.1093/nar/gks1193

Bennett, R. E., Robbins, A. B., Hu, M., Cao, X., Betensky, R. A., Clark, T., . . . Hyman, B. T. (2018). Tau induces blood vessel abnormalities and angiogenesis-related gene expression in P301L transgenic mice and human Alzheimer's disease. *Proc Natl Acad Sci U S A, 115*(6), E1289-E1298. doi:10.1073/pnas.1710329115

Caballero, B., Wang, Y., Diaz, A., Tasset, I., Juste, Y. R., Stiller, B., . . . Cuervo, A. M. (2018). Interplay of pathogenic forms of human tau with different autophagic pathways. *Aging Cell, 17*(1). doi:10.1111/acel.12692

Childs, B. G., Baker, D. J., Wijshake, T., Conover, C. A., Campisi, J., & van Deursen, J. M. (2016). Senescent intimal foam cells are deleterious at all stages of atherosclerosis. *Science, 354*(6311), 472-477. doi:10.1126/science.aaf6659

Coppe, J. P., Patil, C. K., Rodier, F., Krtolica, A., Beausejour, C. M., Parrinello, S., . . . Campisi, J. (2010). A human-like senescence-associated secretory phenotype is conserved in mouse cells dependent on physiological oxygen. *PLoS One, 5*(2), e9188. doi:10.1371/journal.pone.0009188

Correia-Melo, C., Marques, F. D., Anderson, R., Hewitt, G., Hewitt, R., Cole, J., . . . Passos, J. F. (2016). Mitochondria are required for pro-ageing features of the senescent phenotype. *EMBO J, 35*(7), 724-742. doi:10.15252/embj.201592862

de Calignon, A., Spires-Jones, T. L., Pitstick, R., Carlson, G. A., & Hyman, B. T. (2009). Tangle-bearing neurons survive despite disruption of membrane integrity in a mouse model of tauopathy. *J Neuropathol Exp Neurol, 68*(7), 757-761. doi:10.1097/NEN.0b013e3181a9fc66

Dimri, G. P., Lee, X., Basile, G., Acosta, M., Scott, G., Roskelley, C., . . . et al. (1995). A biomarker that identifies senescent human cells in culture and in aging skin in vivo. *Proc Natl Acad Sci U S A, 92*(20), 9363-9367.

Dunckley, T., Beach, T. G., Ramsey, K. E., Grover, A., Mastroeni, D., Walker, D. G., . . . Stephan, D. A. (2006). Gene expression correlates of neurofibrillary tangles in Alzheimer's disease. *Neurobiol Aging, 27*(10), 1359-1371. doi:10.1016/j.neurobiolaging.2005.08.013

Flament, S., Delacourte, A., Verny, M., Hauw, J. J., & Javoy-Agid, F. (1991). Abnormal Tau proteins in progressive supranuclear palsy. Similarities and differences with the neurofibrillary degeneration of the Alzheimer type. *Acta Neuropathol, 81*(6), 591-596.

Frost, B., Bardai, F. H., & Feany, M. B. (2016). Lamin Dysfunction Mediates Neurodegeneration in Tauopathies. *Curr Biol, 26*(1), 129-136. doi:10.1016/j.cub.2015.11.039

Herbig, U., Ferreira, M., Condel, L., Carey, D., & Sedivy, J. M. (2006). Cellular senescence in aging primates. *Science, 311*(5765), 1257. doi:10.1126/science.1122446

Hoover, B. R., Reed, M. N., Su, J., Penrod, R. D., Kotilinek, L. A., Grant, M. K., . . . Liao, D. (2010). Tau mislocalization to dendritic spines mediates synaptic dysfunction independently of neurodegeneration. *Neuron, 68*(6), 1067-1081. doi:10.1016/j.neuron.2010.11.030

Hutter, E., Renner, K., Pfister, G., Stockl, P., Jansen-Durr, P., & Gnaiger, E. (2004). Senescence-associated changes in respiration and oxidative phosphorylation in primary human fibroblasts. *Biochem J, 380*(Pt 3), 919-928. doi:10.1042/BJ20040095

Jurk, D., Wang, C., Miwa, S., Maddick, M., Korolchuk, V., Tsolou, A., . . . von Zglinicki, T. (2012). Postmitotic neurons develop a p21-dependent senescence-like phenotype driven by a DNA damage response. *Aging Cell, 11*(6), 996-1004. doi:10.1111/j.1474-9726.2012.00870.x

Kirkland, J. L., Tchkonia, T., Zhu, Y., Niedernhofer, L. J., & Robbins, P. D. (2017). The Clinical Potential of Senolytic Drugs. *J Am Geriatr Soc, 65*(10), 2297-2301. doi:10.1111/jgs.14969

Kramer, A., Green, J., Pollard, J., Jr., & Tugendreich, S. (2014). Causal analysis approaches in Ingenuity Pathway Analysis. *Bioinformatics, 30*(4), 523-530. doi:10.1093/bioinformatics/btt703

Laurent, C., Buee, L., & Blum, D. (2018). Tau and neuroinflammation: What impact for Alzheimer's Disease and Tauopathies? *Biomed J, 41*(1), 21-33. doi:10.1016/j.bj.2018.01.003

Li, R., & Shen, Y. (2013). An old method facing a new challenge: re-visiting housekeeping proteins as internal reference control for neuroscience research. *Life Sci, 92*(13), 747-751. doi:10.1016/j.lfs.2013.02.014

Makrecka-Kuka, M., Krumschnabel, G., & Gnaiger, E. (2015). High-Resolution Respirometry for Simultaneous Measurement of Oxygen and Hydrogen Peroxide Fluxes in Permeabilized Cells, Tissue Homogenate and Isolated Mitochondria. *Biomolecules, 5*(3), 1319-1338. doi:10.3390/biom5031319

Moritz, C. P. (2017). Tubulin or Not Tubulin: Heading Toward Total Protein Staining as Loading Control in Western Blots. *Proteomics, 17*(20). doi:10.1002/pmic.201600189

Morsch, R., Simon, W., & Coleman, P. D. (1999). Neurons may live for decades with neurofibrillary tangles. *J Neuropathol Exp Neurol, 58*(2), 188-197.

Muir, E. R., Shen, Q., & Duong, T. Q. (2008). Cerebral blood flow MRI in mice using the cardiac-spin-labeling technique. *Magn Reson Med, 60*(3), 744-748. doi:10.1002/mrm.21721

Nilson, A. N., English, K. C., Gerson, J. E., Barton Whittle, T., Nicolas Crain, C., Xue, J., . . . Kayed, R. (2017). Tau Oligomers Associate with Inflammation in the Brain and Retina of Tauopathy Mice and in Neurodegenerative Diseases. *J Alzheimers Dis, 55*(3), 1083-1099. doi:10.3233/JAD-160912

Oddo, S., Caccamo, A., Shepherd, J. D., Murphy, M. P., Golde, T. E., Kayed, R., . . . LaFerla, F. M. (2003). Triple-transgenic model of Alzheimer's disease with plaques and tangles: intracellular Abeta and synaptic dysfunction. *Neuron, 39*(3), 409-421.

Ogrodnik, M., Miwa, S., Tchkonia, T., Tiniakos, D., Wilson, C. L., Lahat, A., . . . Jurk, D. (2017). Cellular senescence drives age-dependent hepatic steatosis. *Nat Commun, 8*, 15691. doi:10.1038/ncomms15691

Orr, M. E., Garbarino, V. R., Salinas, A., & Buffenstein, R. (2015). Sustained high levels of neuroprotective, high molecular weight, phosphorylated tau in the longest-lived rodent. *Neurobiol Aging, 36*(3), 1496-1504. doi:10.1016/j.neurobiolaging.2014.12.004

Orr, M. E., Pitstick, R., Canine, B., Ashe, K. H., & Carlson, G. A. (2012). Genotype-specific differences between mouse CNS stem cell lines expressing frontotemporal dementia mutant or wild type human tau. *PLoS One, 7*(6), e39328. doi:10.1371/journal.pone.0039328

Orr, M. E., Salinas, A., Buffenstein, R., & Oddo, S. (2014). Mammalian target of rapamycin hyperactivity mediates the detrimental effects of a high sucrose diet on Alzheimer's disease pathology. *Neurobiol Aging, 35*(6), 1233-1242. doi:10.1016/j.neurobiolaging.2013.12.006

Orr, M. E., Sullivan, A. C., & Frost, B. (2017). A Brief Overview of Tauopathy: Causes, Consequences, and Therapeutic Strategies. *Trends Pharmacol Sci, 38*(7), 637-648. doi:10.1016/j.tips.2017.03.011

Park, K. H., Hallows, J. L., Chakrabarty, P., Davies, P., & Vincent, I. (2007). Conditional neuronal simian virus 40 T antigen expression induces Alzheimer-like tau and amyloid pathology in mice. *J Neurosci, 27*(11), 2969-2978. doi:10.1523/JNEUROSCI.0186-07.2007

Pesta, D., Hoppel, F., Macek, C., Messner, H., Faulhaber, M., Kobel, C., . . . Gnaiger, E. (2011). Similar qualitative and quantitative changes of mitochondrial respiration following strength and endurance training in normoxia and hypoxia in sedentary humans. *Am J Physiol Regul Integr Comp Physiol, 301*(4), R1078-1087. doi:10.1152/ajpregu.00285.2011

Prins, N. D., & Scheltens, P. (2015). White matter hyperintensities, cognitive impairment and dementia: an update. *Nat Rev Neurol, 11*(3), 157-165. doi:10.1038/nrneurol.2015.10

Rodier, F., Coppe, J. P., Patil, C. K., Hoeijmakers, W. A., Munoz, D. P., Raza, S. R., . . . Campisi, J. (2009). Persistent DNA damage signalling triggers senescence-associated inflammatory cytokine secretion. *Nat Cell Biol, 11*(8), 973-979. doi:10.1038/ncb1909

Salminen, A., & Kaarniranta, K. (2011). Control of p53 and NF-kappaB signaling by WIP1 and MIF: role in cellular senescence and organismal aging. *Cell Signal, 23*(5), 747-752. doi:10.1016/j.cellsig.2010.10.012

Santacruz, K., Lewis, J., Spires, T., Paulson, J., Kotilinek, L., Ingelsson, M., . . . Ashe, K. H. (2005). Tau suppression in a neurodegenerative mouse model improves memory function. *Science, 309*(5733), 476-481. doi:10.1126/science.1113694

Sedelnikova, O. A., Horikawa, I., Zimonjic, D. B., Popescu, N. C., Bonner, W. M., & Barrett, J. C. (2004). Senescing human cells and ageing mice accumulate DNA lesions with unrepairable double-strand breaks. *Nature Cell Biology, 6*(2), 168-170. doi:10.1038/ncb1095

Severino, J., Allen, R. G., Balin, S., Balin, A., & Cristofalo, V. J. (2000). Is beta-galactosidase staining a marker of senescence in vitro and in vivo? *Exp Cell Res, 257*(1), 162-171. doi:10.1006/excr.2000.4875

Seward, M. E., Swanson, E., Norambuena, A., Reimann, A., Cochran, J. N., Li, R., . . . Bloom, G. S. (2013). Amyloid-beta signals through tau to drive ectopic neuronal cell cycle re-entry in Alzheimer's disease. *J Cell Sci, 126*(Pt 5), 1278-1286. doi:10.1242/jcs.1125880

Shen, Q., Huang, S., & Duong, T. Q. (2015). Ultra-high spatial resolution basal and evoked cerebral blood flow MRI of the rat brain. *Brain Res, 1599*, 126-136. doi:10.1016/j.brainres.2014.12.049

Silbert, L. C., Quinn, J. F., Moore, M. M., Corbridge, E., Ball, M. J., Murdoch, G., . . . Kaye, J. A. (2003). Changes in premorbid brain volume predict Alzheimer's disease pathology. *Neurology, 61*(4), 487-492.

Strupp, J. P. Stimulate: A GUI based fMRI Analysis Software Package. *Neuroimage, 3*(3), S607.

Wang, L., Li, C., Sun, Q., Xia, D., & Kao, C. Y. (2009). Active contours driven by local and global intensity fitting energy with application to brain MR image segmentation. *Comput Med Imaging Graph, 33*(7), 520-531. doi:10.1016/j.compmedimag.2009.04.010

Wang, Y., Martinez-Vicente, M., Kruger, U., Kaushik, S., Wong, E., Mandelkow, E. M., . . . Mandelkow, E. (2009). Tau fragmentation, aggregation and clearance: the dual role of lysosomal processing. *Hum Mol Genet, 18*(21), 4153-4170. doi:10.1093/hmg/ddp367

Wegmann, S., Maury, E. A., Kirk, M. J., Saqran, L., Roe, A., DeVos, S. L., . . . Hyman, B. T. (2015). Removing endogenous tau does not prevent tau propagation yet reduces its neurotoxicity. *EMBO J, 34*(24), 3028-3041. doi:10.15252/embj.201592748

Wells, J. A., O'Callaghan, J. M., Holmes, H. E., Powell, N. M., Johnson, R. A., Siow, B., . . . Lythgoe, M. F. (2015). In vivo imaging of tau pathology using multi-parametric quantitative MRI. *Neuroimage, 111*, 369-378. doi:10.1016/j.neuroimage.2015.02.023

Zhu, Y., Tchkonia, T., Pirtskhalava, T., Gower, A. C., Ding, H., Giorgadze, N., . . . Kirkland, J. L. (2015). The Achilles' heel of senescent cells: from transcriptome to senolytic drugs. *Aging Cell, 14*(4), 644-658. doi:10.1111/acel.12344

Acknowledgements. We thank Drs. Jia Nie for assistance with oral gavage; Ning Zang for assistance collecting tissues; and Ji Li for maintaining the mouse colony, assistance with tissue collection and laboratory management. We thank Mr. Anthony Andrade for providing technical assistance with sectioning mouse brains. The Nathan Shock Pathology Core and Nathan Shock Metabolism Core provided the cryostat and Oxygraph-2k, respectively. Drs. Yuji Ikeno and Judith Campisi provided technical advice on SA β–gal staining. We would like to acknowledge Dr. Jonathan Gelfond for assisting with the data analysis, and was supported by NIH grants NIA Shock Center P30AG013319 and NIA Pepper Center P30AG044271. The authors acknowledge Karen H. Ashe for development of the rTg4510 mouse line. We thank the McLaughlin Research Institute: Dr. George Carlson and Rose Pitstick for breeding all mouse lines used here, and Dr. Andrea Grindeland for performing silver staining. We are grateful to the Banner Sun Health Research Institute Brain and Body Donation Program of Sun City, Arizona for the provision of human brain tissue. The Brain and Body Donation Program is supported by the National Institute of Neurological Disorders and Stroke (U24 NS072026 National Brain and Tissue Resource for Parkinson's Disease and Related Disorders, the National Institute on Aging (P30 AG19610 Arizona Alzheimer's Disease Core Center), the Arizona Department of Health Services (contract 211002, Arizona Alzheimer's Research Center), the Arizona Biomedical Research Commission (contracts 4001, 0011, 05-901 and 0110 for the Arizona Parkinson's Disease Consortium) and the Michael J. Fox Foundation for Parkinson's Research. This work was supported by the San Antonio Nathan Shock Center for Excellence, the UT Health Science Center School of Medicine Briscoe Women's Health and the US Department of Veterans Affairs Career Development Award (IK2BX003804) awarded to M.E.O. N.M. is supported by R01-DK80157, R01-DK089229, P30 AG013319 (San Antonio Nathan Shock Center), and P30 AG044271

(San Antonio Claude D. Pepper Older Americans Independence Center). J.M.V. is supported by a Biology of Aging T32 Training Grant (T32 AG021890).

Author Contributions N.M. provided guidance and support to authors and edited the manuscript. J.M.V. designed and conducted GSEA and respirometry experiments, analyzed and interpreted data, prepared figures, wrote methods, independently confirmed key results of gene expression and histological measures, helped write and edit the manuscript. K.S. managed senolytic treatment experiments, performed histological staining, conducted blinded histological analyses of immunofluorescence data, wrote methods and edited the manuscript. E.B. assisted with senolytic treatments, conducted blinded analyses of anatomical MRI images and wrote corresponding methods. Q.S. performed all MRI experiments and analyses, conducted blinded analyses of CBF data and provided oversight to E.B. in anatomical analyses. C.S.T. performed histology, SA β-gal staining and blinded quantification, developed FIJI analysis protocols, wrote methods and edited the manuscript. M.E.O. conceived, supervised and attained funding for the project; designed the experiments, conducted experiments, analyzed and interpreted data, provided guidance and supervision to co-authors, prepared figures and wrote the manuscript.

Conflict of Interest. None Declared

Data Availability Statement. References for source data for Figure 1 are provided with the paper; data that support Figure 1 findings are available from the corresponding author upon reasonable request. All other data supporting the findings of this study are available within the paper, and its extended data files.

Table 1. Human Postmortem Brain Characteristics

	Control (n=10)	PSP (n=14)	p-value
Age at death (yrs)	85.70 ± 2.81	83.86 ± 3.08	0.6765
Sex (M/F)	6/4	9/5	N/A
Last MMSE score	27.67 ± 0.87 (n=9)	21.00 ± 2.02	0.0194
Brain mass (g)	1169 ± 17.83	1139 ± 43.21	0.5800
Total Tangles	4.03 ± 0.77	7.64 ± 0.66	0.0017

Figure 1 | Neurofibrillary tangles were associated with cellular senescence-associated gene pathways in human Alzheimer's disease neurons and tau transgenic mouse brains. (a) Pathways and predicted upstream regulators identified by Ingenuity Pathway Analyses (IPA, QIAGEN) as significantly enriched in Alzheimer's disease patient-derived neurons with neurofibrillary tangles compared to non-tangle containing neurons; z-score plotted on x-axis and (p-value) indicated in bar graph. Cellular functions and (b) predicted upstream regulators employed by neurofibrillary tangle containing neurons derived from Alzheimer's disease patient are shown. (c) Predicted upstream regulators of gene transcription in tau_{NFT} mice after the onset of neurofibrillary tangles (~6-mo-old vs. ~2-mo-old); z-score plotted on x-axis and (p-value) indicated in bar graph. (d-e) Representative immunoblot generated by capillary electrophoresis on chromatin-bound fractions from mouse forebrain homogenate probed with anti-γ-H2ax antibody. (e) Densitometric normalization of γ-H2ax to total protein content (CTL: n=3; tau_{WT} n=4; tau_{NFT}: n=5; ANOVA, *P* = 0.0056. Mice aged 16-18-months old). (f-k) Quantitative gene expression on RNA isolated from CTL (open bar, n=3), tau_{WT} (closed bar, n=3) and tau_{NFT} (red bar, n=4) mouse forebrain

targeting (f): *Cdkn2a, P* = 0.0066 *and* (g) *Cdkn1a, P* = 0.0207. Gene expression was analyzed by one-way ANOVA Tukey's multiple comparison *posthoc*. Data are graphically represented as mean ± s.e.m.

Figure 2 | Neurofibrillary tangles were associated with upregulation of SASP gene expression and NFκB activation. (a) Quantitative gene expression on RNA isolated from CTL (open bar, n=3), tau_{WT} (closed bar, n=3) and tau_{NFT} (red bar, n=4) mouse forebrain targeting SASP associated genes *Il1b, P* = 0.0025; (b) *Cxcl1, P* = 0.0040; (c) *Tnfa*, *P* = 0.0114; (d) *Tlr4*, *P* = 0.0144. (d) Immunoblot generated by capillary electrophoresis on subcellular fractionated mouse forebrain homogenate probed with anti-NFκB p65 antibody. Total cellular p65 (top blot) and nuclear localized p65 protein levels (bottom blot) were (e) normalized to total protein content. Total p65; *P* = 0.0758; nuclear p65, *P* = 0.0223. CTL: open bar, n=3; tau_{WT}: closed bar, n=4; tau_{NFT}: red bar, n=5. In all experiments, mice were aged 16-18-months-old; both males and females were included. Significance determined by one-way ANOVA Tukey's multiple comparison *posthoc*. Data are graphically represented as mean ± s.e.m.

Figure 3 | Brain regions with neurofibrillary tangles displayed altered cellular respiration. (a-c) Representative respirometric traces from cortical and (d-f) hippocampal tissues using the SUIT protocol to measure oxygen consumption (top gray traces: CTL; black middle traces: tau_{WT}; bottom red traces: tau_{NFT}). (g) Tissue mass-specific respiration analyses in cortical and (h) hippocampal tissue. Two-way ANOVA Tukey's multiple comparison *posthoc*: ** $P < 0.005$. (i) Biochemical analyses of citrate synthase (CS) activity to assess total mitochondrial content in the cortex and hippocampus (n=5/group). Experimental mice were aged 16-18-months-old with n=6/group; both males and females were included (j) Total oxygen consumption and (k) *Cdkn2a* gene expression were measured in the cerebellum, a brain region devoid of NFTs. n=3/group. Data are graphically

represented mean ± s.e.m. (ETF_L (fat oxidation in absence of ADP (state 2)), ETF_P (fat oxidation coupled to ATP production), CI_P (complex I activity linked to ATP production (state 3)), CI+CII_P (complex I & II linked respiration (state 3)), CI+CII_E (complex I & II linked respiration uncoupled (maximum respiration), CII_E (complex II activity uncoupled). Data are graphically represented as mean ± s.e.m.

Figure 4 | Senescence-associated *Cdkn2a* was significantly upregulated in mouse and human brains with neurofibrillary tangles and tracked with total tangle deposition and brain atrophy. (a) Genetically ablating endogenous mouse tau to significantly reduce neurofibrillary tangle load results in concomitant 60% reduction in *Cdk2na* expression (two-tailed t-test: t = 5.903, df = 4, P = 0.0041; n=3/group) and (b) significant reduction in brain atrophy (two-tailed t-test, P = 0.0143; n =3/group). (c) Tracking *Cdkn2a* expression in tau_{WT} mice reveals a significant age-dependent increase (one-way ANOVA: $F(2, 6) = 15.44$, P = 0.0043; n = 3/group for tau_{WT} and n=4 tau_{P301L}). In contrast to significantly lower expression than tau_{NFT} mice at 16-month-old (P = 0.0075), Dunnett's multiple comparison test indicates that at 22-months of age, tau_{WT} mouse *Cdkn2a* expression is no longer statistically lower than tau_{NFT} mice (P = 0.0577) and by 28-30 months they are statistically the same (P = 0.999). (d) Immunofluorescence and Bielschowsky silver staining revealed neurofibrillary tangles in 18-mo-old tau_{WT} mouse hippocampal CA1 (NeuN, neuron, green; PHF1: phosphorylated tau, red; DAPI, blue, nuclei). (d) qPCR analyses of RNA extracted from 3xTgAD mice with Aβ plaques is compared to tau_{NFT} set at y = 1. 3xTgAD *Cdkn2a* expression is no different than age-matched C57BL/6 mice (two-tailed t-test, t = 1.784, df = 9, P = 0.1081; n = 3 WT, n = 6 3xTgAD; n = 4 tau_{NFT}). Both mouse cohorts express significantly less *Cdkn2a* than tau_{NFT} mice (one-way ANOVA: $F(2, 12) = 43.25$; $P < 0.0001$). (f) *Cdkn2a* expression level is significantly correlated with brain atrophy (R^2 = 0.5615, $P <$ 0.0001; n = 43). (g) qPCR analyses of RNA extracted from brains from control older adult humans (n=10; ave. age = 85.70yrs) and age-matched progressive supranuclear palsy

(n=14; ave. age = 83.86yrs) indicate a 57% upregulation of *CDKN2A* with progressive supranuclear palsy diagnosis (unpaired t-test, t = 2.165, df = 22, *P* = 0.0415) that (h) positively correlates with neurofibrillary tangle deposition in the parietal lobe (ANOVA, *P* = 0.0008; Kendall's Tau rank correlation *P* = 0.059). (i) Immunoblot generated by capillary electrophoresis on cortical brain homogenate from control and progressive supranuclear palsy human brains probed with total tau antibody, HT7. The individual with the highest *CDKN2A* expression (panel g) displayed high molecular weight tau, lane 9*. Data is graphically represented as error bars, mean ± s.e.m.

Figure 5 | Senolytic treatment reduced neurofibrillary tangle burden, ventricular enlargement and neurodegeneration in 23-month-old tau transgenic mice. (a) Representative brain images analyzed for neurofibrillary tangles in tau transgenic mice treated with either vehicle or dasatinib and quercetin (DQ). (Phosphorylated tau, PHF1, red; total tyrosine phosphorylation, pTyr, yellow; and DAPI nuclei; blue. Scale bar = 10μm). (b) Neurofibrillary tangle counts from n = 3 mice/group sampled from 12 cortical images/mouse and analyzed with unpaired two-tailed t-test, **** *P* < 0.0001. (c) DQ significantly reduced hippocampal *Tlr4, P* = 0.0459, and *Cxcl1, P* = 0.0142*,* gene expression as measured by qPCR. Vehicle-treated (open symbols, n=7) and DQ-treated (red closed symbols, n = 5); data analyzed by unpaired two-tailed t-test. (d) Representative brain images from anatomical T2-weighted MRI. (e) Quantification of ventricle volume analyzed by one-way ANOVA, *P* = 0.0010; Holm-Sikak's *posthoc:* *** *P* = 0.0007, * *P* = 0.05. (f) Immunoblot generated by capillary electrophoresis on forebrain homogenates (n = 6/group) with antibodies against neuronal proteins NeuN, synaptophysin (synapto.), and PSD95 normalized to total protein. (g) Neuronal protein expression was normalized to total protein and analyzed by unpaired two-tailed t-test, NeuN: * *P* = 0.0432, (h) synaptophysin (Synapto): * *P* = 0.0416 and (i) PSD95: * *P* = 0.0398. n = 6/group. Data represented as mean +/- SEM.

Supporting Data Figure 1 | The tau_{NFT} mouse model develops neurofibrillary tangles and brain atrophy. (a-c) Histological staining of cortical brain sections from 16-month-old (a) CTL, (b) tau_{WT} and (c) tau_{NFT} mice with antibodies against neurons (NeuN, red); neurofibrillary tangles (PHF1, green) and nuclei (DAPI, blue). Only tau_{NFT} mice develop neurofibrillary tangles at this age. Scale bar 10μm. (d) Histological comparison of CTL hemibrain (left) to tau_{NFT} mouse hemibrain (right). Images illustrate severe forebrain atrophy with ventricular enlargement in tau_{NFT} mice. (e) Brain weight measurements reflect the significant neurodegeneration in tau_{NFT} mice (n=3/group; one-way ANOVA: P = 0.0015, Tukey's posthoc analysis: CTL vs. tau_{WT} = 0.0644, CTL vs. tau_{NFT} = 0.0011; tau_{WT} vs. tau_{NFT} = 0.0477. Data are graphically represented as mean ± s.e.m. (f-i) Quantitative gene expression analyses on RNA isolated from CTL non-transgene expressing littermates of tau_{WT} mice (TRE- tau_{WT}: closed circles) and tau_{NFT} mice (TRE-tau_{NFT}: red circles) mouse forebrain indicates statistically similar expression by unpaired two-tailed t-test. (f) *Tnfa*: P = 0.2256 (g) *Tlr4*: P = 0.5230 (h) *Il1b*: P = 0.2244 and (i) *Cxcl1:* P = 0.9808. Data are graphically represented as mean with 95% CI.

Supporting Data Figure 2 | The tau-induced senescence-associated gene expression was dependent on high molecular weight tau. (a) Sixteen-month-old tau_{WT} and tau_{NFT} mice express similar levels of *Mapt* gene expression. (b) Representative capillary electrophoresis immunoblot using total human tau antibody (HT7) on brain homogenates from 16-mo-old tau_{WT} and tau_{NFT} mice. (c-g) Quantitative gene expression analyses on RNA isolated from control (CTL, non-transgene expressing mice), tau_{WT} and tau_{NFT} mice. (c) Some senescence-associated genes were not changed by NFT formation (i.e., (c) *Il6* or (d) *Lmnb1*). The significant upregulation in other senescence-associated genes in tau_{NFT} but not tau_{WT} mice allowed us to identify a gene expression array dependent on NFT formation. These genes include *Tnfa, Tlr4, Il1β, Cxcl1, Cdk1a and Cdkn2a*. Gene expression was normalized to neuronal *Mapt* expression and analyzed by Two-way ANOVA. N=3/mice

group. (f-g) *Cdkn1a* and *Cdkn2a* are reproducibly elevated in a separate mouse cohort. Unpaired two-tailed t-test: *Cdkn1a*: *P* = 0.0086 and (g) *Cdkn2a*: *P* = 0.0016; tau_{NFT} mice (closed bars) and CTLs (TRE-tau_{NFT}: open bars); n=3/group).

Supporting Data Figure 3 | Senescence associated beta galactosidase reactivity was positively correlated with brain mass, but not neurofibrillary tangle pathology. (a) Senescence associated beta galactosidase (SA β-gal) staining carried out at pH 6.0 illustrated reactivity in 1-mo-old control mouse forebrain and (b) cerebellum. (c) Quantitative gene expression analyses on RNA isolated from CTL (open bar), tau_{WT} (closed bar) and tau_{NFT} (red bar) mouse forebrain revealed significantly upregulated lysosomal hydrolase *Glb1* gene expression in tau_{NFT} mice; ANOVA, *P* = 0.0070; CTL: n=3; tau_{WT} n=3; tau_{NFT}: n=4. (d) SA β-gal staining of control 18-mo-old brain; CA1 (box) and cortex (brackets). (e) Tau_{NFT} mouse brains stained with β-galactosidase developed very low reactivity at pH 6.0 but (f) positive β-galactosidase activity was observed in tau_{NFT} mice when stained at physiological pH 4. (g-h) Immunostaining with anti-NeuN revealed co-labeling of SA β-gal positive cells with neurons. (i) Five experimental cohorts of CTL, tau_{WT} and tau_{NFT} 18-mo-old mice were analyzed for SA β-gal reactivity at pH 6.0; both males and females were included. The number of CA2 cells sampled on each histological slide was plotted; (j) the total number of CA2 cells counted did not differ among genotypes. (k) The percentage of SA β-gal positive CA2 cells was significantly lower in tau_{WT} mice than controls, and tau_{NFT} mice contained significantly fewer SA β-gal positive CA2 cells than CTL and tau_{WT} mice. (Repeated measures one-way ANOVA: *P* = 0.0049). (l) The percentage of SA β-gal positive CA2 cells was significantly correlated with brain mass (R^2 = 0.4852, *P* = 0.0 039). Data are graphically represented as mean ± s.e.m.

Supporting Data Figure 4 | Genetically ablating endogenous mouse tau reduced production of SASP. Quantitative gene expression analyses on RNA isolated from tau_{NFT} mice on a *Mapt* wild type background (closed bars) and *Mapt* knockout background (hatched bars) mouse forebrain revealed a reduction in (a) *Tnfa*, $P = 0.0047$; (b) *Il1b,* $P = 0.0949$; (c) *Cxcl1,* $P = 0.0559$; and (d) *Tlr4,* $P = 0.1494$. N=3/group were analyzed by unpaired two-tailed t-test. Data are graphically represented as mean ± s.e.m.

Supporting Data Figure 5 | Senolytic treatment provided modest benefits to brain structure and function in an advanced stage tauopathy mouse model. (a) Whole brain, cortex and subcortex brain volume quantification from anatomical T2-weighted MRI of tau_{NFT} $Mapt^{0/0}$ mice (shown in Figure 4). Mice received senolytic treatment (dasatinib (D) and quercetin (Q), DQ, n=6) or vehicle (n=8) for three months and were compared to non-transgenic $Mapt^{0/0}$ mice (n=3). Data were analyzed with two-way ANOVA, Tukey's *posthoc:* * $P < 0.05$; ** $P < 0.005$). (b) Representative brain images illustrating areas of white matter hyperintensity (WMH, yellow pixels) were (c) analyzed by one-way ANOVA, $P = 0.0330$; Tukey's *posthoc* * $P = 0.0291$. (d) Representative MRI cerebral blood flow images. (e) MRI quantification of cerebral blood flow of whole brain, cortex and subcortical brain regions. Two-way ANOVA treatment main effect, $P = 0.0057$; Tukey's *posthoc:* * $P = 0.0141$. (f) Composite analysis of tau_{NFT} + vehicle and tau_{NFT} + DQ MRI data analyzed by two-way ANOVA DQ treatment main effect: * $P = 0.0138$. (Tau_{NFT} + vehicle, n=8; tau_{NFT} + DQ, n=6; non-transgenic, n=3; all mice were on a $Mapt^{0/0}$ background).

Supporting Data Figure 6 | Senolytic treatment decreased SASP gene expression but not astrocytes or microglia. (a) Quantitative senescence gene expression array from hippocampus of vehicle-treated (open symbols, n=7) and DQ-treated (red closed symbols, n = 5) mice relative to neuronal *Mapt* gene expression. Two-way ANOVA: treatment main effect, ***P = 0.0006. (b) Representative capillary electrophoresis immunoblot using antibodies against GFAP and Iba1 to quantify relative levels of astrocytes and microglia, respectively, in brain homogenates from vehicle or senolytic (dasatinib and quercetin, DQ) treated mice. (c) Densitometric normalization of GFAP and (d) Iba1 antibody immunoreactivity against total protein analyzed by unpaired two-tailed t-test. ** = 0.0013. N=6/group Data are graphically represented as mean ± s.e.m.

Supporting Data Figure 7 | Senolytic treatment did not alter soluble tau expression. (a) Representative capillary electrophoresis immunoblot using total human tau antibody (HT7) on brain homogenates from vehicle or senolytic (dasatinib and quercetin, DQ) treated mice. (b) Densitometric normalization of total tau immunoreactivity against total protein indicates similar protein expression between treatment groups. Vehicle, n=5; DQ, n=4. Data are graphically represented as mean with 95% CI.

Supporting Data Figure 8 | Total protein concentration was used as the internal loading control for protein quantification. (a) Representative capillary electrophoresis immunoblot on cytosolic (Cyt.) and nuclear (Nuc.) enriched fractions using antibodies against Lamin A/C and β-Actin. (b) Representative capillary electrophoresis immunoblot of brain homogenates from control or tau transgenic mice using antibodies against Lamin A/C and β-Actin. (c) Representative capillary electrophoresis immunoblot used to detect total protein concentration. (d) Quantification of Lamin A/C, (e) β-Actin and (f) total protein

concentration. CTL: n = 3; tau_{NFT}: n = 5; unpaired two-tailed t-test, Lamin A/C **** P < 0.0001; β–Actin: ** P = 0.0097; Total Protein: P = 0.2916. (g) Representative electropherogram generated from capillary electrophoresis total protein immunoblot.

Figure 1 | Neurofibrillary tangles were associated with cellular senescence-associated gene pathways in human Alzheimer's disease neurons and tau transgenic mouse brains.

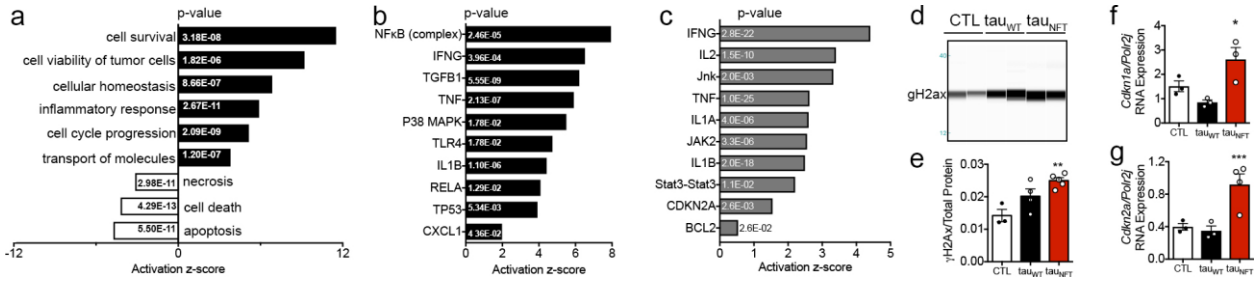

Figure 2 | Neurofibrillary tangles were associated with upregulation of SASP gene expression and NFκB activation

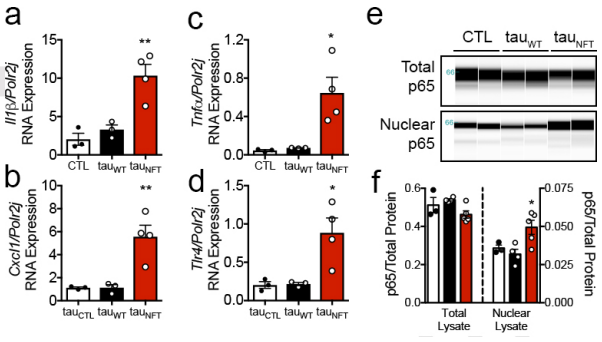

Figure 3 | Neurofibrillary tangle-containing brain regions displayed impaired cellular respiration.

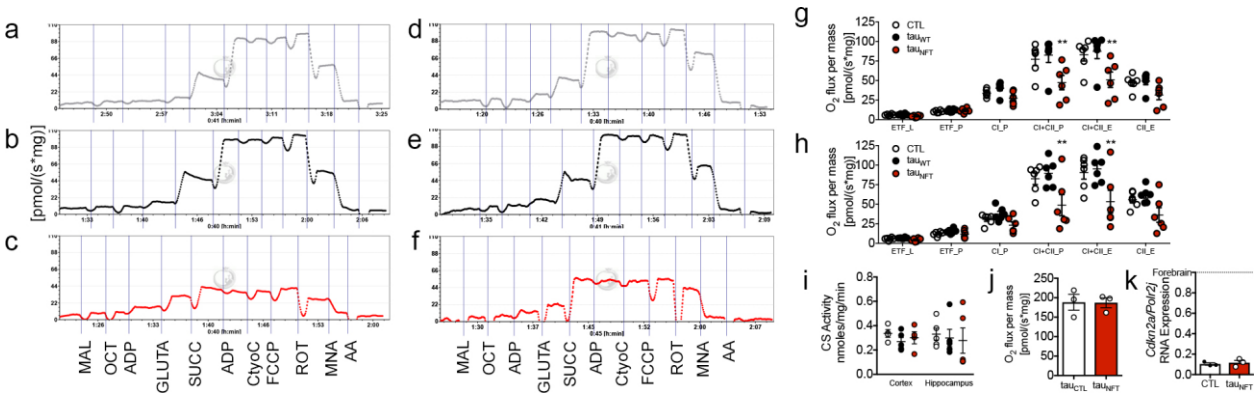

Figure 4 | Senescence-associated *Cdkn2a* was significantly upregulated in mouse and human brains with neurofibrillary tangles and tracked with total tangle deposition and brain atrophy.

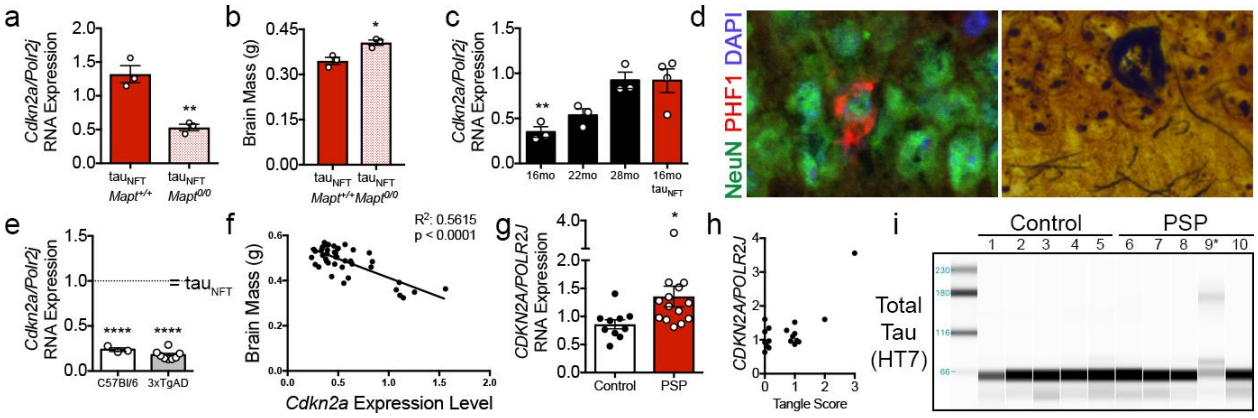

Figure 5 | Senolytic treatment reduced NFT burden, ventricular enlargement and neurodegeneration in 23-month-old tau transgenic mice.